Nanoscale

Accepted Manuscript

This article can be cited before page numbers have been issued, to do this please use: L. Zhao, J. Wang, D. Su, Y. Zhang, H. Lu, Y. Xu, J. Bai, Y. Gao and G. Lu, *Nanoscale*, 2020, DOI: 10.1039/D0NR05649A.

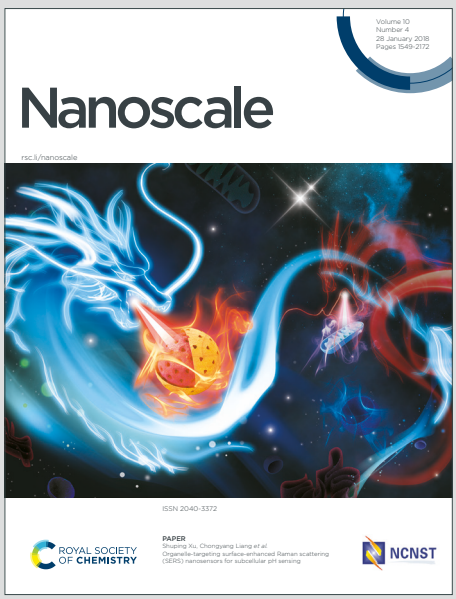

ROYAL SOCIETY OF CHEMISTRY

rsc.li/nanoscale

View Article Online
DOI: 10.1039/D0NR05649A

DNA controllable peroxidase mimetic activity of MoS_2 nanosheets for constructing robust colorimetric biosensor

Lianjing Zhao, Jing Wang, Dandan Su, Yueying Zhang, Huiying Lu, Xu Yan,* Jihao Bai, Yuan Gao* and Geyu Lu*

State Key Laboratory on Integrated Optoelectronics, College of Electronic Science and Engineering, Jilin University, 2699 Qianjin Street, Changchun 130012, China

*Corresponding authors:

Xu Yan, Tel.: +86 431 85167808

Email: yanx@jlu.edu.cn (X. Yan)

Yuan Gao, Tel.: +86 431 85168384;

Email: gaoyuan@jlu.edu.cn (Y. Gao).

Geyu Lu, Tel.: +86 431 85167808;

Email: lugy@jlu.edu.cn (G. Lu).

View Article Online
DOI: 10.1039/D0NR05649A

Abstract

The low activity of nanozymes that work as a candidate of natural enzyme limits their applications in the fabrication of biosensor, drawing increasing attention in improving their catalytic capacity. In this work, the peroxidase-like activity of MoS_2 nanosheets (NSs) was dramatically enhanced through DNA modification, which was 4.3-times higher than that of bare MoS_2 NSs. Such an enhancement of catalytic activity was mainly ascribed to the increased affinity of DNA/MoS_2 NSs toward substrate TMB, further accelerating electron transfer from TMB to H_2O_2. On the base of DNA tuned MoS_2 NSs nanozyme activity, a colorimetric sensing platform was developed for facile detection of carcinoembryonic antigen (CEA) in a sensitive manner. Interestingly, a convenient, affordable and instrument-free portable test kit was fabricated to visually monitor CEA by rooting aptamer/MoS_2 NSs system into agarose hydrogel. Importantly, our work illuminates the feasibility of using DNA to enhance catalysis of nanozymes and their application potential for label-free, portable and visual detection of aptamer targeted biomolecules.

Keywords: MoS_2 nanosheets, DNA, peroxidase-like activity, tumor biomarker

View Article Online
DOI: 10.1039/D0NR05649A

Introduction

As direct surrogate of natural enzymes, nanozymes exist multivalent elements or hold mimicking catalytic sites of natural enzymes, capturing tremendous attention because of multiple advantages of cost effectiveness, bulk-preparation, easy-modification and excellent stability.[1, 2] Nowadays, many nanomaterials such as metal oxides nanoparticles (Fe_3O_4, CeO_2 and Co_3O_4 nanoparticles), carbon nanomaterials (carbon dots and graphene), noble metals and two dimensional transition metal dichalcogenides (2D TMDs) have been reported to possess enzyme mimetic activity.[3-13] One challenge in the field of nanozymes research is that nanomaterials possess intrinsic weaker catalytic activities in comparation with nature enzymes, limiting the scope and performance of their applications.[14-16] Thus, it remains a significant challenge to obtain nanozymes with robust catalytic activity. To enhance the catalytic activities of nanozymes, quite a few efforts have been dedicated to fabricating hybrid nanostructures, surface modification of nanozymes or combining nanozymes with natural enzymes.[17-21] Among those strategies, surface modification of nanozymes arouses growing attention owing to its ease of operation. Studies has demonstrated that DNA modification can obviously enhance enzyme-mimicking activity of Fe_3O_4 nanoparticles (NPs), graphitic carbon nitride nanosheets (NSs) and Au NPs, attributed to the enhanced affinity of theses nanozyme to substrate.[22-26] In contrast, the catalytic activity of CeO_2 NPs was distinctly inhibited after addition of DNA due to electrostatic interactions between positively charged TMB and negatively charged DNA or physical hindrance blocking the accessibility of substrate to nanoparticles.[4, 27] This implies that employing nucleic acid to regular catalysis of sensitized nanozymes may be an effective approach, which will extend nanozymes applications in the fields of sensing, imaging and therapeutic areas.

MoS_2 NSs, as a representative of 2D TMD, have gained burgeoning interests in sensor and biomedical applications during the past several years due to unique optical properties, capacity of loading large amounts of biomolecules and good biocompatibility.[28-31] Recently, it is discovered that MoS_2 NSs possess intrinsic

peroxidase-like activity.[32] Some researches described that MoS_2 NSs can adsorb polymers and then their enzyme mimicking activity is improved due to the change of interface property.[33] MoS_2 NPs modified with negatively charged polymers present a better catalysis, compared with bare or positive-charged polymers modified MoS_2 NPs.[34] As a polymer with negative charge, single-strand DNA (ssDNA) can be adsorbed by MoS_2 NSs,[35] which may be an effective enhancer of catalysis of MoS_2 NSs. Nevertheless, biointerface interaction between DNA and MoS_2 NSs as well as the mechanism of DNA modification impact on enzyme-like activity of MoS_2 NSs are scarcely studied systematically.

In this contribution, the catalytic activity of MoS_2 NSs was significantly enhanced through DNA modification. The interaction among MoS_2 NSs, ssDNA and TMB were systematically investigated to illustrate the mechanism of enhancement of catalysis. The enhanced catalytic activity mainly resulted from the improved affinity of DNA/MoS_2 NSs to peroxidase substrate TMB rather than hydroxyl radicals generation. Carcinoembryonic antigen (CEA) aptamer is a short ssDNA with high affinity and specificity for target protein CEA, which is selected by exponential enrichment (SELEX) method in vitro. Furthermore, aptamer controllable enzyme-mimetic activity of MoS_2 NSs was employed to construct a colorimetric biosensor for label-free detection of tumor biomarker. In the presence of CEA, CEA aptamer would preferentially bind with CEA and desorb from the surface of MoS_2 NSs, resulting in the decrease of catalysis activity. As a result, UV-vis absorbance of TMB-H_2O_2 system decreased, accompanying the change of solution color. On the base of recording absorbance, the strategy of sensitive detection of CEA was developed. Furthermore, portable test kits for visually detecting CEA was fabricated by using agarose hydrogel as a robust solid supporter to hold aptamer/MoS_2 NSs system. This novel sensing platform is not only simple in design, but also does not comprise oligonucleotide labeling and elaborate nanomaterials modification process.

Experimental

View Article Online
DOI: 10.1039/D0NR05649A

Materials and apparatus

3,3′,5,5′-Tetramethylbenzidine (TMB), Terephthalic acid (TA) and 5,5-dimethyl-1-pyrroline *N*-oxide (DMPO) were purchased from Sigma Aldrich. Carcinoembryonic antigen (CEA), alpha fetoprotein (AFP) and mucin-1(muc-1) were purchased from Shanghai Linc-Bio Science Co., Ltd. MoS_2 (NSs) nanosheets were obtained from Nanjing XF Nano Material Tech Co., Ltd. All oligonucleotide sequences used in the present work were synthesized and purified by Sangon BiotechCo., Ltd. The sequence of Cy5 labeled DNA is 5'- cyanine dye Cy5-ATACCAGCTTATTCAATT. The sequence of CEA aptamer (CA) is 5'-ATACCAGCTTATTCAATT-3'. The electron spin resonance (ESR) spectra were obtained on a JES-FA 200 EPR spectrometer. Cyclic voltammetric measurement of bare or MoS_2 NSs modified electrodes was carried out on a CHI760E electrochemical workstation (Chenhua, China). The high solution transmission electron microscope (HRTEM) image of MoS_2 NSs was acquired on a JEOL TEM-3010 instrument.

Peroxidase activity assay

The peroxidase-like activities of MoS_2 NSs and aptamer modified MoS_2 NSs (aptamer/MoS_2 NSs) were evaluated through catalyzing oxidation of TMB in the presence of H_2O_2. Aptamer/MoS_2 NSs were prepared by mixing 20 μM aptamer with 200 μg/mL MoS_2 NSs and incubating for 10 minutes at room temperature. Subsequently, the hybrid of 5 μg/mL aptamer/MoS_2 NSs or 5 μg/mL MoS_2 NSs in 0.1M acetate buffer (pH 4.0) was mixed with 0.2 mM H_2O_2 and 0.4 mM TMB. After 15 minutes incubation at 37 ºC, the UV-Vis absorbance spectrum was recorded immediately.

Detection of hydroxyl radicals by terephthalic acid

The detection of hydroxyl radicals by Terephthalic acid (TA) was performed as follow: 1 mM TA, 0.2 mM H_2O_2 and various concentrations of MoS_2 NSs or aptamer/MoS_2 NSs were added in 0.1 M sodium acetate buffer (pH 4.0), followed by 12 hours incubation in the dark at room temperature. The fluorescence spectra were measured under light excitation at 315 nm.

View Article Online
DOI: 10.1039/D0NR05649A

Carcinoembryonic antigen detection

Carcinoembryonic antigen (CEA) detection was carried out as follows: the mixture of different concentrations of CEA and 5 μg/mL aptamer/MoS_2 NSs in 10 mM Tris-HCl buffer was incubated at 37 ºC for 30 minutes. Then the above reaction mixture was added in 0.1M acetate buffer (pH 4.0) containing 0.2 mM H_2O_2 and 0.4 mM TMB. After 15 minutes incubation at 37 ºC, the UV-vis absorption spectrum was determined immediately.

Results and discussion

Enhancement of catalytic activity of MoS_2 NSs

We started our investigation with the characterization of MoS_2 NSs. The transmission electron microscopy (TEM) image showed that the MoS_2 possessed a two-dimensional nanosheet structure with the average diameter of about 75 nm (Fig. 1A). The single-strand DNA (ssDNA) adsorption on the MoS_2 NSs was validated by the measurement of fluorescence spectra. As illustrated in Fig. 1B, cyanine dye Cy5 labeled ssDNA emitted intense fluorescence at 665 nm. The fluorescence signal was completely quenched by MoS_2 NSs after 10 min incubation, indicating the adsorption of ssDNA on the surface of MoS_2 NSs. The adsorption was also evidenced in the zeta potentials studies afterwards. Subsequently, the peroxidase-like activity of MoS_2 NSs and ssDNA/MoS_2 NSs hybrid (DNA/MoS_2 NSs) was evaluated via TMB/H_2O_2 system. As displayed in Fig. 1C, in the absence of nanozyme, TMB/H_2O_2 system shows negligible absorbance at 652 nm (curve a), indicated that little TMB oxidation product (TMBox) is produced. The color of reaction solution is close to colorless (photo a). MoS_2 NSs can catalyze TMB oxidation in the presence of H_2O_2, producing a moderate absorbance peak at 652 nm (curve c) and presenting tinged blue (photo c). In comparison, DNA/MoS_2 NSs exhibit robust catalytic activity, proved by the obviously enhanced absorbance signal (curve d) and visual bright blue of reaction solution (photo d). Noting that the catalytic activity of MoS_2 NSs with modification of ssDNA was 4.3-

fold higher than that of bare MoS_2 NSs. On the other hand, there was no obvious difference in the absorbance intensity between TMB/H_2O_2/DNA system (curve b) and TMB/H_2O_2 system, indicating that ssDNA itself does not catalyze the reaction. It was observed that the enhancement of peroxidase-like activity of MoS_2 NSs was proportional to the concentration of ssDNA (Fig. 1D). The signal began to increase slowly when ssDNA concentration was over 500 nmol/L. The effect of base composition and length of ssDNA on the catalysis of MoS_2 NSs were ascertained by measuring the catalytic activity of MoS_2 NSs modified with different sequence of ssDNA. As shown in Fig. 1E, catalytic activity of 20 bp homo ssDNA (A_{20}, C_{20}, G_{20} and T_{20}) modified MoS_2 NSs follows the trend of $G_{20} \approx T_{20} > A_{20} > C_{20}$ > no DNA. This could originate from the difference in the interaction between different bases and TMB. C_{20} modified MoS_2 NSs displayed the weakest activity among four polynucleotides. The p*K*a of cytosine is 4.5. Most of them is protonated in the buffer at pH 4, which may lead to a lower affinity of MoS_2 NSs nanozyme to TMB and related lower catalysis due to electrostatic repulsion between cytosine and positively charged TMB. As presented in Fig. 1F, longer ssDNA has a stronger ability to enhance enzyme mimetic activity of MoS_2 NSs among poly Tn (n=5, 10, 15, 20, 30, 40) modified MoS_2 NSs when total concentration of nucleosides was fixed. The optimal sequence length was approximate 30 nucleotide. Longer ssDNA can be adsorbed more readily by MoS_2 NSs because of a stronger interaction between MoS_2 NSs and longer ssDNA.

The influence of temperature, pH and buffer type on the catalytic capacity of nanozyme was further explored. Reaction temperature also influenced the enzymatic activity of both bare MoS_2 NSs and DNA/MoS_2 NSs, which was gradually enhanced with the increase of temperature in the range from 25 ºC to 55 ºC (Fig. 1G). By contrast, previous research reported that the catalysis of natural horseradish peroxidase (HRP) decreases obviously when temperature was over 40 ºC. Therefore, both MoS_2 NSs and DNA/MoS_2 NSs nanozymes can extend application of nanozymes over a wide temperature range. The catalysis of MoS_2 NSs and DNA/MoS_2 NSs depended on solution pH as well. The highest peroxidase-like activity of DNA/MoS_2 NSs was achieved at pH 4, in good accordance with that of MoS_2 NSs (Fig. 1H). Subsequently,

the buffer whose pH range includes 4 was chosen to explore the effect of buffer on the catalysis of nanozyme. By comparison, the absorbance at 652 nm of reaction systems in NaAc-HAc buffer at pH 4 was distinctly higher than those in sodium citrate-citric acid buffer and Na_2HPO_4-HAc buffer at pH 4 (Fig. 1I), revealing the TMB/H_2O_2 reaction system has a higher catalytic activity in NaAc-HAc buffer.

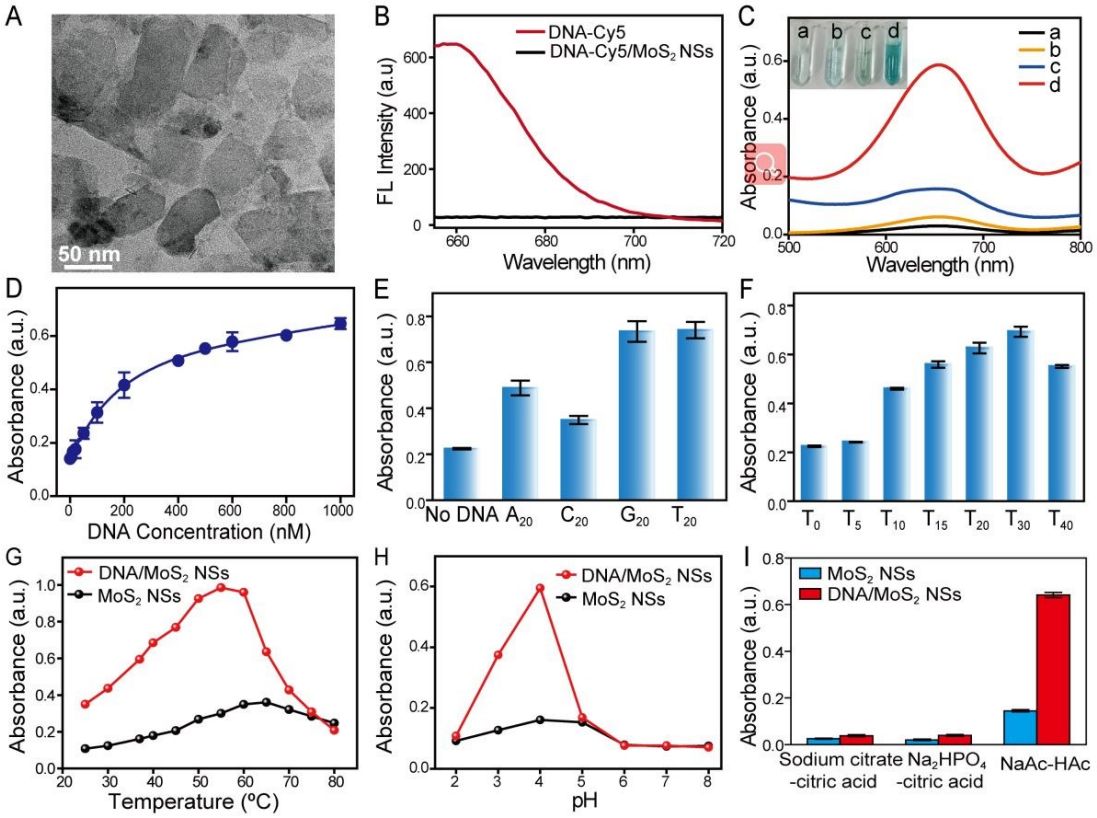

Fig. 1 (A) TEM image of MoS_2 NSs. (B) Fluorescent spectra of Cy5 labeled DNA with and without MoS_2 NSs. The concentration of ssDNA and MoS_2 NSs is 75 nmol/L and 15 μg/mL, respectively. (C) The absorbance spectra of different reaction systems. Inset of (C) shows visible color of different reaction systems: a TMB/ H_2O_2, b TMB/H_2O_2/DNA, c TMB/H_2O_2/MoS_2 NSs, d TMB/H_2O_2/DNA/MoS_2 NSs. (D) The change of UV-vis absorbance at 652 nm with different DNA concentrations. The effect of base composition (E) and sequence length (F) of DNA on the peroxidase-like activity of MoS_2 NSs. The effect of temperature (G), pH (H) and buffer (I) on the peroxidase-like activity of MoS_2 NSs and DNA/MoS_2 NSs.

Mechanism of DNA enhancing activity of MoS_2 NSs nanozyme

To better understand the mechanism of activity enhancement of MoS_2 NSs nanozyme after addition of ssDNA, catalytic mechanism of MoS_2 NSs was first investigated. According to previous studies, the possible catalytic mechanism of nanozymes with peroxidase-like activity is mainly divided into two classes, the generation of hydroxyl radicals and electron transfer process.[10, 36, 37] To confirm the type of catalytic mechanism of MoS_2 NSs, the electron spin resonance (ESR) spectrum determination were performed to directly detect whether or not hydroxyl radicals was generated. The 5,5-dimethyl-1-pyrroline N-oxide (DMPO) was adopted as a hydroxyl radicals scavenger to form DMPO/•OH spin adduct, which presented four characteristic peaks with relative intensities of 1 : 2 : 2 : 1. As displayed in Fig. 2A, the obvious ESR signal of DMPO/•OH spin adduct was observed in the presence of Fe^{2+} and H_2O_2, indicating the generation of hydroxyl radicals from H_2O_2 decomposition. Whereas no ESR signal of DMPO/•OH spin adduct was recorded during the interaction of MoS_2 NSs and H_2O_2, suggested no hydroxyl radicals generation. Noting that the catalytic mechanism of MoS_2 NSs was different from Fenton reaction, excluding the possibility of catalysis caused by hydroxyl radicals. Hydroxyl radicals formation was further monitored by fluorescence assay, where terephthalic acid (TA) was applied as a sensitive fluorescence probe for tracking hydroxyl radicals. TA can react with H_2O_2 and generate 2-hydroxy terephthalic acid (TAOH), which emitted a maximum fluorescence peak at 430 nm upon excitation of 315 nm light. As shown in Fig. 2B, the sample only containing TA and H_2O_2 has a strong fluorescence signal at 430 nm, revealing hydroxyl radicals formation. However, the fluorescence intensity gradually decreased with the addition of increased concentrations of MoS_2 NSs, demonstrated that MoS_2 NSs prevent hydroxyl radicals generation, further eliminating the probability of catalytic mechanism triggered by hydroxyl radicals. Then the other catalytic mechanism about electron transfer process was taken into consideration. To estimate the ability of MoS_2 NSs to facilitate electron transfer, the electrocatalytic behaviors of bare and MoS_2 NSs modified glass carbon electrode to reduce H_2O_2 were measured by cyclic voltammetry. As seen in Fig. 2C, almost no electrochemical signal was observed on the bare electrode but a strong electrochemical signal was obtained on the MoS_2 NSs modified electrode.

This result reveals that MoS_2 NSs exhibit electrocatalytic activity during the reduction of H_2O_2, which verifies that MoS_2 NSs possess the capacity of accelerating electron transfer between electron donor (electrode) and electron acceptor (H_2O_2). Based on the above analysis, it is thought that MoS_2 NSs exert their catalytic activity in TMB-H_2O_2 reaction through accelerating electron transfer between TMB and H_2O_2. It is worth to mention that ESR signal of DMPO/•OH spin adduct was not observed in the present of DNA/MoS_2 NSs and H_2O_2 (Fig. 2A). Moreover, the fluorescence intensity at 430 nm further decreased with the addition of DNA/MoS_2 NSs, compared with that of MoS_2 NSs (Fig. 2B). Both of the results demonstrate that DNA/MoS_2 NSs can not catalyze H_2O_2 decomposition to generate hydroxyl radicals. Thus, it is proposed that the mechanism of activity enhancement primarily arises from further accelerated electron transfer process rather than hydroxyl radicals generation as well.

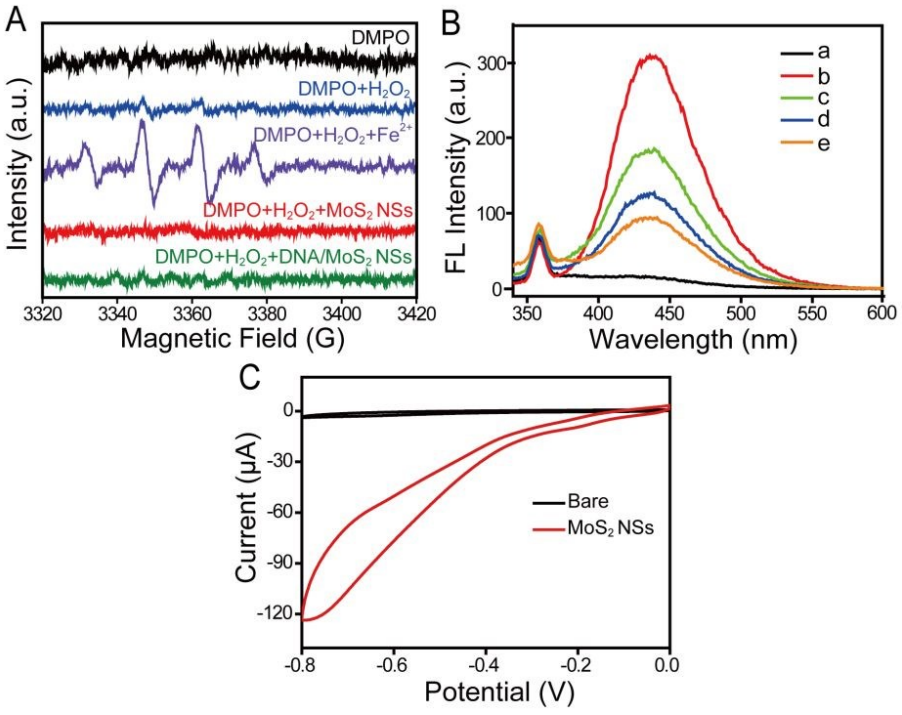

Fig. 2 (A) ESR signal of DMPO/•OH spin adduct of different reaction systems. (B) Fluorescence spectra for interaction of TA with H_2O_2, MoS_2 NSs and DNA/MoS_2 NSs. a TA, b TA+H_2O_2, c TA+H_2O_2+MoS_2 NSs 1a, d TA+H_2O_2+MoS_2 NSs 5a, e TA+H_2O_2+DNA+MoS_2 NSs 5a, a=0.5 μg/mL. (C) Cyclic voltammograms of bare electrode and MoS_2 NSs modified electrode.

The steady state kinetics assay was conducted to further elucidate the mechanism

of catalysis enhancement by keeping the concentration of TMB or H_2O_2 constant. As shown in Fig. 3, typical Michaelis-Menten Curves were obtained for both TMB and H_2O_2. The steady state kinetics parameters, the maximum reaction velocity (V_{max}) and Michaelies constant (K_m), were calculated by lineweaver-burk plot, $1/\upsilon = (K_m/V_{max}) \times (1/[s]) + 1/V_{max}$. K_m approximatively indicates the affinity of enzyme to substrate. The K_m value of DNA/MoS_2 NSs using TMB as substrate is 4.6-times lower than that of MoS_2 NSs, suggesting that the affinity of MoS_2 NSs to TMB is substantially enhanced after modifying ssDNA (Table S1). The high affinity can further promote the contact of active sites of MoS_2 NSs with substrate TMB, accelerating the electron transfer between them and enhancing the catalysis of MoS_2 NSs.[38] This is consist with the results of above mechanism study, where activity enhancement mainly originates from the accelerated electron transfer process. While the K_m value of DNA/MoS_2 NSs using H_2O_2 as substrate is 6 times higher than that of MoS_2 NSs, illuminated that ssDNA modification only enhances the affinity of MoS_2 NSs to TMB.

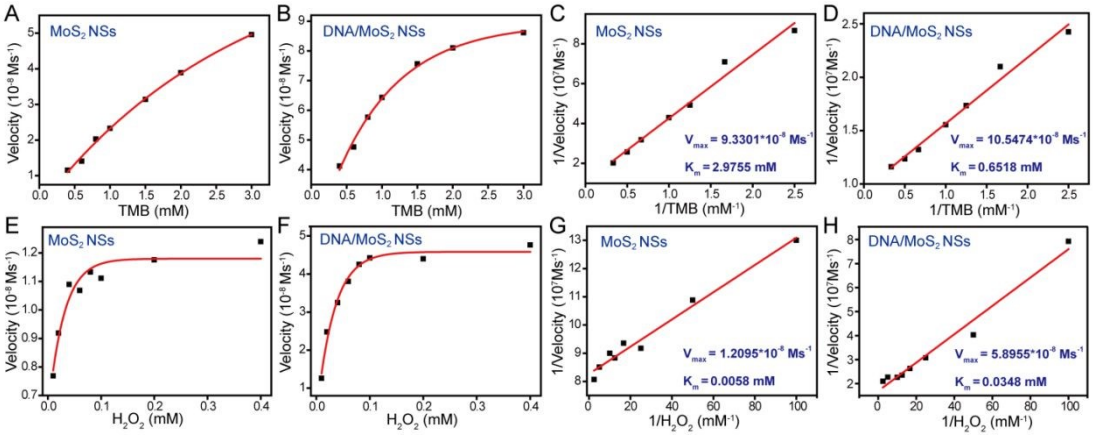

Fig. 3 Steady state kinetic assay of MoS_2 NSs (A and E) and DNA/MoS_2 NSs (B and F) and Double-reciprocal plots of the catalytic activity of bare MoS_2 NSs (C and G) and DNA/MoS_2 NSs (D and H) with the concentration of TMB and H_2O_2 fixed, respectively.

Subsequently, more attention was paid on the interaction among MoS_2 NSs, ssDNA and TMB. The above fluorescence experiment demonstrated that MoS_2 NSs could adsorb ssDNA. To ascertain the type of intermolecular forces which played a predominant role in ssDNA adsorption by MoS_2 NSs, ssDNA adsorption and desorption experiments were carried out (detailed process is presented in

supporting information). As exhibited in Fig. 4A, more and more fluorescence signal is quenched by MoS_2 NSs as salt concentration gradually increases, because the electrostatic repulsion between ssDNA and MoS_2 NSs was overcome. Fig. 4B reveals that the addition of guanosine does not trigger desorption of ssDNA from MoS_2 NSs, implying that nucleobases seldom participate in the ssDNA adsorption. Besides, only a small portion of ssDNA desorption emerged after adding phosphate, NaOH, DMSO and Urea. DMSO and Urea were separately utilized to disrupt hydrophobic interactions and hydrogen bonding. These results indicated that ssDNA adsorption was influenced by pH of solution, ssDNA phosphate backbone, hydrophobic interactions and hydrogen bonding but they played a little rather than major role in ssDNA adsorption. Afterward, ssDNA desorption was induced by surfactants with different molecule weigh. The high molecular weight surfactants (0.01% Tween 20 and 0.01% Triton) could detach more ssDNA from MoS_2 NSs than small molecular weight surfactants (0.01% CTAB and 0.01% SDS) (Fig. 4C). This is in good accordance with that the higher molecular weight surfactant has a stronger van der Waals force. Thus, van der Waals force, a ubiquitous intermolecular force, is believed to be primary surface force for ssDNA adsorption by MoS_2 NSs, after ruling out other intermolecular forces. Identical conclusion is obtained by theoretical work regarding intermolecular force of DNA and MoS_2 NSs.[39] Zeta potential of MoS_2 NSs changed from -19.2 mV to -36 mV after addition of ssDNA, also illustrating the adsorption of ssDNA on the MoS_2 NSs (Fig. 4D). Both MoS_2 NSs and DNA/MoS_2 NSs are less negatively charged after addition of TMB, suggesting the adsorption of TMB on the surface of MoS_2 NSs and DNA/MoS_2 NSs. The DNA/MoS_2 NSs with more negative charge possess a stronger electrostatic attraction to TMB than that of bare MoS_2 NSs, increasing the affinity of MoS_2 NSs to TMB. Consequently, the enzymatic activity of MoS_2 NSs was enhanced and electron transfer rate between TMB and MoS_2 NSs was accelerated. This is supported by aforementioned steady state kinetics assay, where the affinity of MoS_2 NSs to substrate TMB was dramatically enhanced after addition of ssDNA. If the substrate TMB was substituted with a negative charged

substrate, 2,2'-azino-bis(3-ethylbenzothiazoline-6-sulfonic acid) diammonium salt (ABTS), the catalysis of DNA/MoS_2 NSs was distinctly inhibited on account of the reduced affinity, resulting from electrostatic repulsion between ABTS and ssDNA adsorbed on the surface of MoS_2 NSs (Fig. 4E). The experiment result demonstrated the electrostatic interaction between substrate and modification on the surface of MoS_2 NSs had great impact on the enzymatic activity of MoS_2 NSs again. The conclusion was further verified by comparing peroxidase-like activity of MoS_2 modified with various charged polymers. As displayed in Fig. 4F, the negatively charged polymers, ssDNA and polystyrene sulfonate (PSS), modified MoS_2 NSs had a higher catalysis than bare MoS_2 NSs. In comparison with bare MoS_2 NSs, the positively charged polyethyleneimine (PEI) and uncharged Polyvinyl Pyrrolidone (PVP) modified MoS_2 NSs separately presented a lower and negligibly changed catalysis. Among them, only negatively charged polymers could distinctly improve catalytic activity of MoS_2 NSs and ssDNA was the most effective enhancer.

On the basis of above analysis, the mechanism of ssDNA enhancing peroxidase-like activity of MoS_2 NSs is deemed as follows (Fig. 4G). First, ssDNA was adsorbed on the surface of MoS_2 NSs via van der Waals force and then obviously increased electrostatic attraction between MoS_2 NSs and TMB, leading to distinct enhancement of the affinity between them. The improved affinity could promote the contact of active sites of MoS_2 NSs with substrate TMB, further accelerating electron transfer from lone-pair electrons in TMB amino groups to MoS_2 NSs. Subsequently, electron density and mobility of MoS_2 NSs were enhanced, resulting in the acceleration of electron transfer from MoS_2 NSs to H_2O_2. As a result, the electron transfer process from TMB to H_2O_2 catalyzed by MoS_2 NSs was obviously accelerated via adding ssDNA.

It was reported that H_2O_2 can efficiently displace DNAs adsorbed by CeO_2 NPs due to the strong affinity between H_2O_2 and CeO_2 NPs.[12] To ascertain whether H_2O_2 and TMB could displace DNAs adsorbed by MoS_2 NSs, different concentrations of H_2O_2 and TMB were added into the mixture of Cy5 labeled ssDNA and MoS_2 NSs where all fluorescence of Cy5 labeled ssDNA could be almost quenched by MoS_2 NSs.

As shown in Fig. S1, even the addition of higher concentration of H_2O_2 or TMB, there is no obvious fluorescence recovery, suggesting that H_2O_2 and TMB do not trigger DNA desorption from the surface of MoS_2 NSs.

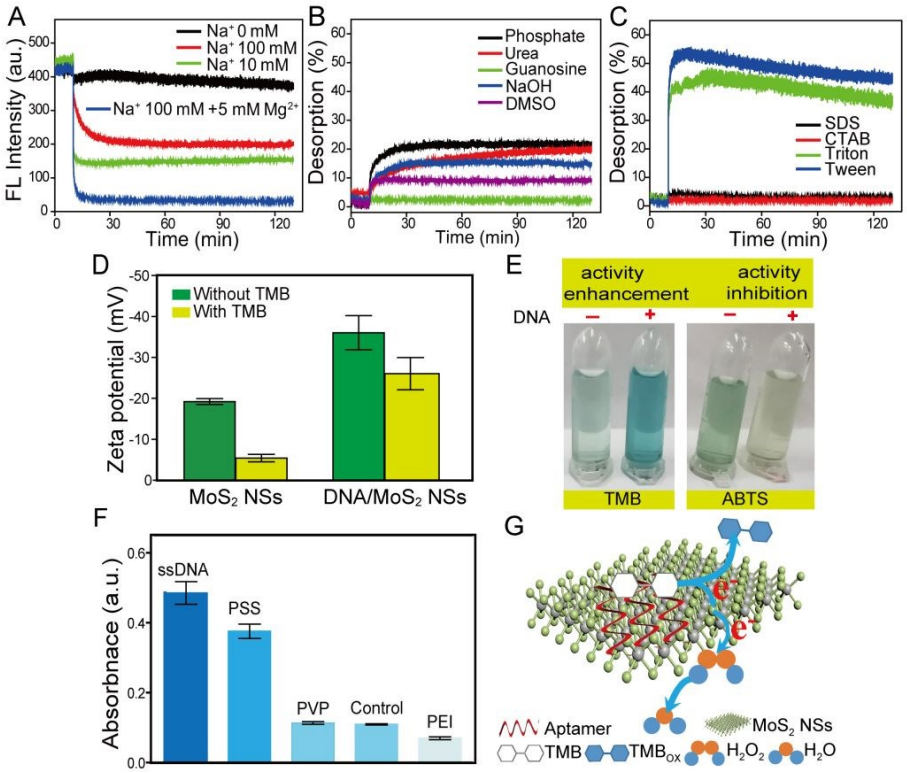

Fig. 4 (A) Kinetics of Cy5 labeled DNA adsorption by MoS_2 NSs at different salt concentration. Kinetics of Cy5 labeled DNA desorption from MoS_2 NSs after adding (B) different chemicals and (C) different Surfactants. (D) Zeta potential of MoS_2 NSs and DNA/MoS_2 NSs with and without TMB. (E) Photograph of catalytic oxidation of TMB and ABTS by bare MoS_2 NSs or DNA/MoS_2 NSs in the presence of H_2O_2. (F) Comparison of peroxidase-like activity of MoS_2 NSs modified with various charged polymers. (G) Proposed catalytic mechanism of DNA/MoS_2 NSs.

Fabrication of sensing platform

Taking the favorable capacity of MoS_2 NSs into account, it is expected that the MoS_2 NSs could be served as signal amplifier to construct a colorimetric sensing platform for accurate and reliable tracing biomarker. CEA as one of the most common tumor biomarkers, has been used in clinical diagnosis and prognosis of various gastroenteric tumor.[40-42] So facile and cost-effective strategy for monitoring CEA is of great

significance for early diagnosis and treatment of multiple tumor. Additionally, aptamers as promising alternative of antibody are attractive for the construction of biosensor owing to their good stability, ease of synthesis and modification, low cost and low toxicity. Thus, the sensing platform based on the CEA aptamer controllable peroxidase-like activity of MoS_2 NSs was developed for label-free detection of CEA, as illustrated in Scheme 1. MoS_2 NSs have a weak intrinsic catalytic activity for TMB-H_2O_2 reaction system. After addition of CEA aptamer, they can be adsorbed by MoS_2 NSs and significantly enhance peroxidase-like activity of MoS_2 NSs. As expected, the absorbance signal of reaction solution is enhanced and the color of the solution turns dark blue. However, if CEA protein exists in the solution, aptamer will preferentially bind with CEA, detaching from the surface of MoS_2 NSs, leading to the decrease of catalytic activity of MoS_2 NSs. As a result, the color of reaction system will become lighter with the increase of CEA concentration. Thus, a colorimetric strategy for label-free detection of CEA is developed on the basis of the recognition function of aptamer and its adjustment function for catalysis of MoS_2 NSs nanozymes.

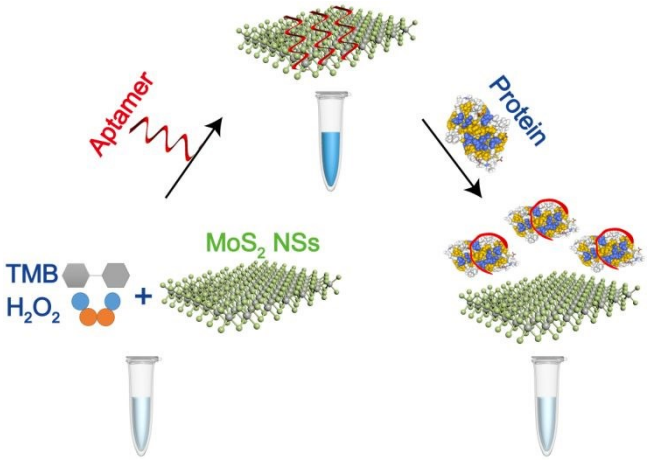

Scheme 1 Schematic illustration of colorimetric biosensor based on aptamer modified MoS_2 NSs for CEA protein detection.

Feasibility of the proposed DNA/MoS_2 NSs based sensing platform for CEA detection was verified. As presented in Fig. 5A, the UV-vis absorbance of TMB/H_2O_2/MoS_2 NSs system is hardly affected by addition of CEA protein. While the absorbance was dramatically enhanced after addition of CEA aptamer. As expected, the absorbance reduced after addition of CEA in the TMB/H_2O_2/aptamer/MoS_2 NSs system.

This was due to the fact that the strong interaction between CEA and its aptamer triggered aptamer desorption from the surface of MoS_2 NSs, decreasing the enzymatic activity of aptamer/MoS_2 NSs. Aptamer desorption was also proved by the measurement of fluorescence spectra. The quenched fluorescence signal of CEA aptamer probe by MoS_2 NSs was restored after adding CEA, suggesting aptamer desorption from the surface of MoS_2 NSs (Fig. S3).

The sensing platform based on the aptamer/MoS_2 NSs was employed to detect CEA protein. As shown in Fig. 5B, the UV-vis absorbance intensity at 652 nm of reaction system gradually decreases with the increasing CEA concentration from 0 to 1000 ng/mL. Simultaneously, corresponding color of the solution changes from dark blue to tinged blue as increased concentration of CEA (inset of Fig. 5B). Fig. 5C reveals that CEA concentration linearly responds to the absorbance of TMBox in the range of 50-1000 ng/mL with the detection limit of 50 ng/mL (S/N=3). The regression equation is $Abs = 0.436-2.773\times10^{-4}[CEA]$, R=0.993.

The specificity of the constructed biosensor was evaluated by investigating the response of biosensor for interferences, containing possible co-existing two kinds of tumor biomarker, alpha fetoprotein (AFP) and mucin-1(muc-1), two common protein, bovine serum albumin (BSA) and immunoglobulins G (IgG), some common amino acids and metal ions. Fig. 5D displayed the absorbance change of the proposed biosensor after addition of interferences under the same procedure. Compared to significant absorbance change after adding CEA (500 ng/mL), the absorbance intensity of the system showed negligible or little change after adding other proteins (500 ng/mL), amino acid (5 μg/mL) and metal ion (5 μg/mL), demonstrating the excellent specificity of the proposed biosensor. In addition, specificity of the biosensor for two reducing substance, cysteine (Cys) and glutathione (GSH) was estimated. As shown in Fig. S2, compared with CEA (500 ng/mL), the sensing platform exhibits similar response for high concentrations of Cys and GSH (5 μg/mL), indicating the constructed biosensor has weak anti-interference capacity for high concentrations of reductant. This is probably because the reductant inhibits peroxidase-like activity of nanozyme. Actually, the concentration of reductant we chose is obviously higher than those in serum. In the

followed standard addition experiment, determined concentration of CEA-spiked in three diluted serum samples was close to the added concentration, indicating the potential of the biosensor for practical application.

The potential of the fabricated biosensor for practical application was verified through standard addition method. Table 1 exhibits that the determined concentration of CEA-spiked in three diluted serum samples is close to the added concentration. The recovery rate of CEA-spiked in serum samples ranges from 91.0% -113.7%, indicating the promising application of the proposed biosensor in complex sample. To further explore the feasibility of point-of-care detection of tumor biomarker, a portable test kit for visual detection of CEA was designed as a proof-of-concept. Agarose hydrogel was chosen as solid supporter owing to its large loading capacity, low cost and negligible background color. As displayed in Fig. 5E, the color of hydrogel changes with the increasing concentration of CEA in the range of 100-3000 ng/ml. The higher concentration of CEA, the lighter is the color of the hydrogel. The result demonstrates the promising application potential of aptamer/MoS_2 NSs nanozymes in preparing portable test kits for tumor biomarker detection.

View Article Online
DOI: 10.1039/D0NR05649A

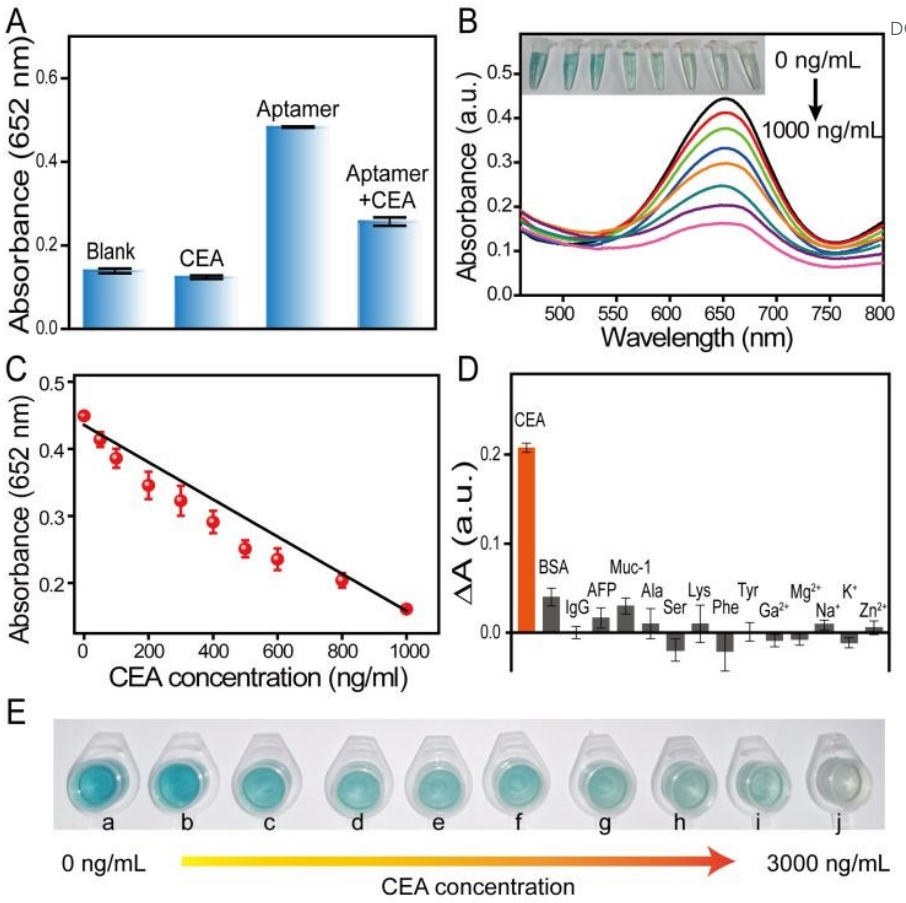

Fig. 5 (A) The UV-vis absorbance at 652 nm of TMB-H_2O_2 reaction catalyzed by bare MoS_2 NSs or aptamer/MoS_2 NSs in the absence or presence of CEA. (B) UV-vis spectra of colorimetric detection of CEA based on aptamer/MoS_2 NSs. The inset presents corresponding images. (C) The linear calibration curve for CEA detection. (D) Specificity of the proposed biosensor based on the aptamer/MoS_2 NSs. (E) The images of hydrogel with different concentrations of CEA when opening the snap cap of portable test kit. The corresponding concentration of CEA from a to j is 0, 100, 200, 400, 600, 800, 1000, 1500, 2000, 3000 ng/mL, respectively.

Table 1. The fabricated sensing platform for CEA detection in serum sample.

Samples	Added (ng/mL)	Found (ng/mL)	Recovery (%)	RSD (%)
Serum 1	500	565.9 ±17.0	113.7	3.4
Serum 2	500	532.9 ± 21.2	106.6	4.2
Serum 3	500	455.1 ± 55.0	91.0	11

View Article Online
DOI: 10.1039/D0NR05649A

Conclusion

In summary, the catalytic mechanism of MoS_2 NSs nanozyme could be attributed to the acceleration of electron transfer from TMB to H_2O_2. After ssDNA modification, the peroxidase-like activity of MoS_2 NSs was significantly enhanced for 4.3-fold. The enhancement mainly originates from the improved affinity of MoS_2 NSs to substrate TMB, which can further facilitate the electron transfer process. Taking advantage of DNA-controllable nanozyme activity, a label-free sensing platform based on the aptamer/MoS_2 NSs was established for CEA detection, displaying sensitive recognition in ng/mL level. Furthermore, such a good sensing platform was successfully loaded on agarose hydrogel to fabricate convenient portable test kit for visually monitoring of CEA. This work provides a facile approach to enhance catalytic activity of nanozyme and affords a promising sensing platform for portable detection of tumor biomarker.

Conflicts of interest

There are no conflicts to declare.

Acknowledgments

This work was supported by grants from the National Nature Science Foundation of China (61304242, 61520106003) and China Postdoctoral Science Foundation (No. 2018M640282).

View Article Online
DOI: 10.1039/D0NR05649A

References

1. D. Jiang, D. Ni, Z. T. Rosenkrans, P. Huang, X. Yan and W. Cai, *Chem. Soc. Rev.*, 2019, **48**, 3683-3704.
2. J. Wu, X. Wang, Q. Wang, Z. Lou, S. Li, Y. Zhu, L. Qin and H. Wei, *Chem. Soc. Rev.*, 2019, **48**, 1004-1076.
3. Z. Zhang, X. Zhang, B. Liu and J. Liu, *J. Am. Chem. Soc.*, 2017, **139**, 5412-5419.
4. R. Pautler, E. Y. Kelly, P.-J. J. Huang, J. Cao, B. Liu and J. Liu, *ACS Appl. Mater. Interfaces*, 2013, **5**, 6820-6825.
5. J. Dong, L. Song, J.-J. Yin, W. He, Y. Wu, N. Gu and Y. Zhang, *ACS Appl. Mater. Interfaces*, 2014, **6**, 1959-1970.
6. K. Fan, J. Xi, L. Fan, P. Wang, C. Zhu, Y. Tang, X. Xu, M. Liang, B. Jiang, X. Yan and L. Gao, *Nat. Commun.*, 2018, **9**, 1440.
7. Y. Song, K. Qu, C. Zhao, J. Ren and X. Qu, *Adv. Mater.*, 2010, **22**, 2206-2210.
8. M. S. Hizir, M. Top, M. Balcioglu, M. Rana, N. M. Robertson, F. Shen, J. Sheng and M. V. Yigit, *Anal. Chem.*, 2016, **88**, 600-605.
9. A. P. Nagvenkar and A. Gedanken, *ACS Appl. Mater. Interfaces*, 2016, **8**, 22301-22308.
10. T. M. Chen, X. J. Wu, J. X. Wang and G. W. Yang, *Nanoscale*, 2017, **9**, 11806-11813.
11. L. Gao, J. Zhuang, L. Nie, J. Zhang, Y. Zhang, N. Gu, T. Wang, J. Feng, D. Yang and S. Perrett, *Nat. Nanotechnol.*, 2007, **2**, 577-583.
12. W. Zhang, W. Zhu, S. Shi, N. Hu, Y. Suo and J. Wang, *J. Mater. Chem. A*, 2018, **6**, 16220-16227.
13. S. Shi, W. Zhang, X. Ren, M. Li, J. Sun, G. Li, Y. Wang, T. Yue and J. Wang, *Carbohyd. Polym.*, 2019, **226**, 115283.
14. H. Cheng, L. Zhang, J. He, W. Guo, Z. Zhou, X. Zhang, S. Nie and H. Wei, *Anal. Chem.*, 2016, **88**, 5489-5497.
15. W. Zhang, S. Li, X. Liu, C. Yang, N. Hu, L. Dou, B. Zhao, Q. Zhang, Y. Suo and J. Wang, *Adv. Funct. Mater.*, 2018, **28**, 1706375.
16. X. Liu, L. Huang, Y. Wang, J. Sun, T. Yue, W. Zhang and J. Wang, *Sens. Actuators B Chem.*, 2020, **306**, 127565.

17. Y. Guo, L. Deng, J. Li, S. Guo, E. Wang and S. Dong, *ACS Nano*, 2011, **5**, 1282-1290.
18. H. Wang, S. Li, Y. Si, N. Zhang, Z. Sun, H. Wu and Y. Lin, *Nanoscale*, 2014, **6**, 8107-8116.
19. Y. Zhang, Z. Zhou, F. Wen, J. Tan, T. Peng, B. Luo, H. Wang and S. Yin, *Sens. Actuators B Chem.*, 2018, **275**, 155-162.
20. B. Liu and J. Liu, *Nano Research*, 2017, **10**, 1125-1148.
21. L. Huang, K. Chen, W. Zhang, W. Zhu, X. Liu, J. Wang, R. Wang, N. Hu, Y. Suo and J. Wang, *Sens. Actuators B Chem.*, 2018, **269**, 79-87.
22. B. Liu and J. Liu, *Nanoscale*, 2015, **7**, 13831-13835.
23. Y.-M. Wang, J.-W. Liu, G. B. Adkins, W. Shen, M. P. Trinh, L.-Y. Duan, J.-H. Jiang and W. Zhong, *Anal. Chem.*, 2017, **89**, 12327-12333.
24. M. Yin, S. Li, Y. Wan, L. Feng, X. Zhao, S. Zhang, S. Liu, P. Cao and H. Wang, *Chem. Commun.*, 2019, **55**, 12008-12011.
25. Y. Hua, M. Liu, S. Li, F. Liu, Y. Cai, H. Liu, Y. Wan, X. Lv and H. Wang, *Biosens. Bioelectron.*, 2019, **124-125**, 89-95.
26. S. Li, X. Zhao, X. Yu, Y. Wan, M. Yin, W. Zhang, B. Cao and H. Wang, *Anal. Chem.*, 2019, **91**, 14737-14742.
27. M. I. Kim, K. S. Park and H. G. Park, *Chem. Commun.*, 2014, **50**, 9577-9580.
28. K. Kalantar-zadeh, J. Z. Ou, T. Daeneke, M. S. Strano, M. Pumera and S. L. Gras, *Adv. Funct. Mater.*, 2015, **25**, 5086-5099.
29. C. Zhu, Z. Zeng, H. Li, F. Li, C. Fan and H. Zhang, *J. Am. Chem. Soc.*, 2013, **135**, 5998-6001.
30. T. Liu, C. Wang, X. Gu, H. Gong, L. Cheng, X. Shi, L. Feng, B. Sun and Z. Liu, *Adv. Mater.*, 2014, **26**, 3433-3440.
31. L. Zhao, M. Cheng, G. Liu, H. Lu, Y. Gao, X. Yan, F. Liu, P. Sun and G. Lu, *Sens. Actuators B Chem.*, 2018, **273**, 185-190.
32. W. Yin, J. Yu, F. Lv, L. Yan, L. R. Zheng, Z. Gu and Y. Zhao, *ACS Nano*, 2016, **10**, 11000-11011.
33. J. Yu, D. Ma, L. Mei, Q. Gao, W. Yin, X. Zhang, L. Yan, Z. Gu, X. Ma and Y. Zhao, *J. Mater. Chem. B*, 2018, **6**, 487-498.

View Article Online
DOI: 10.1039/D0NR05649A

34. K. Zhao, W. Gu, S. Zheng, C. Zhang and Y. Xian, *Talanta*, 2015, **141**, 47-52.
35. J. Shi, J. Lyu, F. Tian and M. Yang, *Biosens. Bioelectron.*, 2017, **93**, 182-188.
36. H. Su, D.-D. Liu, M. Zhao, W.-L. Hu, S.-S. Xue, Q. Cao, X.-Y. Le, L.-N. Ji and Z.-W. Mao, *ACS Appl. Mater. Interfaces*, 2015, **7**, 8233-8242.
37. Vinita, N. R. Nirala and R. Prakash, *Sens. Actuators B Chem.*, 2018, **263**, 109-119.
38. Y. Zhu, S. Murali, W. Cai, X. Li, J. W. Suk, J. R. Potts and R. S. Ruoff, *Adv. Mater.*, 2010, **22**, 5226-5226.
39. H. Vovusha and B. Sanyal, *RSC Adv.*, 2015, **5**, 67427-67434.
40. N. Beauchemin and A. Arabzadeh, *Cancer Metast. Rev.*, 2013, **32**, 643-671.
41. J. Sun, X. Cai, M. M. H. Yung, W. Zhou, J. Li, Y. Zhang, Z. Li, S. S. Liu, A. N. Y. Cheung, H. Y. S. Ngan, Y. Li, Z. Dai, Y. Kai, A. Tzatsos, W. Peng, D. W. Chan and W. Zhu, *Oncogene*, 2019, **38**, 564-580.
42. Z. Wang, N. Liu, F. Feng and Z. Ma, *Biosens. Bioelectron.*, 2015, **70**, 98-105.

View Article Online
DOI: 10.1039/D0NR05649A

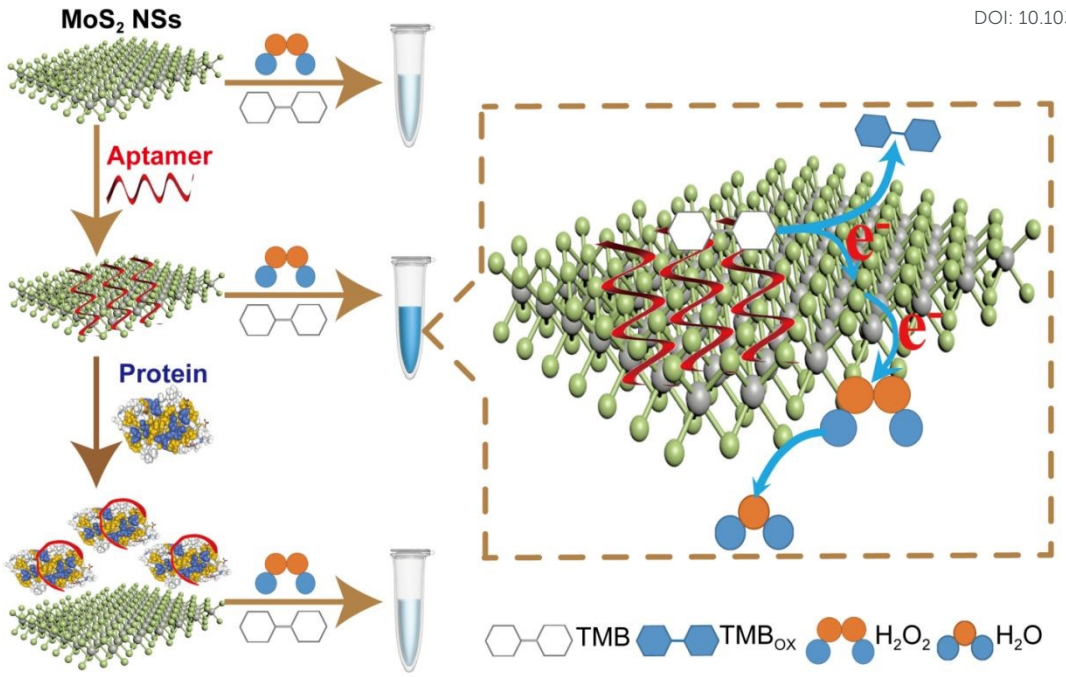

Robust colorimetric biosensor for label-free detection of CEA based on DNA controllable peroxidase mimetic activity of MoS_2 nanosheets